Asian Journal of Chemistry; Vol. 32, No. 11 (2020), 2934-2942

ASIAN JOURNAL OF CHEMISTRY

https://doi.org/10.14233/ajchem.2020.22971

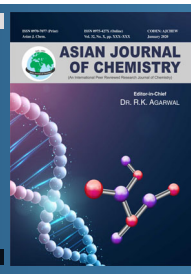

Plant Mediated Synthesis of Zinc Oxide Nanoparticles and their Potential Applications as Photocatalyst and Antibacterial Agents

A. SWETHARANYAM[1], R. KUNJITHAM[1,*] and JUHI BARNWAL[2]

[1]P.G. & Research department of Chemistry, Poompuhar College (Autonomous), (Affiliated to Bharathidasan University, Tiruchirappalli), Melaiyur-620024, India
[2]Department of Chemistry, Ranchi University, Ranchi-834002, India

*Corresponding author: E-mail: kunjithamr@gmail.com

Received: 28 August 2020; *Accepted*: 4 October 2020; *Published online*: 28 October 2020; AJC-20120

In present work, two different methods (sol-gel and biological) were adopted for synthesis of ZnO nanoparticles. The synthesized ZnO nanoparticles were characterized for its optical, structural, photocatalytic, biological activities. Both synthesized nanoparticles demonstrated a wurtzite hexagonal structure. The morphological analysis revealed that most of the nanoparticles are of spherical shape. The photocatalytic activity of the synthesized ZnO nanoparticles was determined through the degradation of acid black 1 dye in which the biosynthesized ZnO NPs provided good performance as compared to that the chemically synthesized ZnO NPs. Furthermore, antibacterial activity, the zone of inhibition of bacterial growth was higher in the biosynthesized ZnO NPs and also antioxidant activity.

Keywords: ZnO nanoparticles, Photocatalytic activity, Acid black 1 dye, Antibacterial activity.

INTRODUCTION

One of the most in depth semi-conductor style metal oxides for research is zinc oxide (ZnO). ZnO has a large band gap of approximately 3.37 eV among semiconductor materials as well as an exaction energy binding 60 meV and Wurtzite structure [1]. In wurtzite, Zn exists where the anion is bordered by four cations at the corners of tetrahedron and *vice-versa*. This tetrahedral coordination is founded on the characteristic of sp^3 covalent bonding nature. In the crystal structure of ZnO, the wurtzite structure has a hexagonal structure with two lattice parameters, a and c [2]. The ZnO semiconductors have received enormous attention due to their distinct and desirable applications in diverse area of chemistry, physics, biology, medicine and electron properties of zinc oxide include an elevated charge transfer, a large difference between emission and absorption, high compound stability and high photostability [3].

Much attention has been directed to the biosynthesis of inorganic nanoparticles using biomaterials as reducing and stabilizing agents due to the non-toxic, eco-friendly and safe reagents used during the biosynthesis process. Moreover, the chemical methods such as co-precipitation, hydrothermal and sol-gel techniques have been used for the synthesis of ZnO nanoparticles [4]. By using chemical reductions these nanoparticles give good results as a cost-effective protective agent against hazardous agents. In recent years, the green synthesis system has had various advantages, especially the use of eco-friendly, low cost, simple and biocompatible materials. Muthuvel *et al*. [5] reported that the biosynthesized ZnO NPs established an effective photocatalytic and antibacterial activity against various pathogens. The synthesis of ZnO NPs using different plants such as *Aloe vera* [6], *Azadirachta indica* [7], *Vitex negundo* [8], *Moringa oleifera* [9], *Hibiscus rosa sinensis* [10] *etc*., have also been previously reported.

ZnO nanoparticles are efficient alternative for photocatalytic degradation of dyes and other environmental pollutants [11]. Therefore, the present study interesting to synthesized ZnO NPs by green method using *Trianthema portulacastrum* and *Mollugo oppositifolia* leaf extract. *T. portulacastrum* and *M. oppositifolia* is a very common and easily available weed in India. It has biomedical properties and its production needs no investment. Another reason is that there are some active components that can help in the synthesis of nanoparticles. In this present work, chemically and biological synthesis and

characterizations of prepared ZnO NPs. The synthesized nanoparticles characterizations by XRD, FT-IR, HR-TEM, UV-DRS and PL measurements were presented. Furthermore both synthesized nanoparticles evaluated by photocatalytic, antibacterial and antioxidant activities are studied.

EXPERIMENTAL

Zinc nitrate, sodium borohydride, organic dye *viz*. acid black 1 was procured from Sigma-Aldrich, India while different reagents were of analytical grade and purchased from different standard chemical companies. Deionized water was used throughout the experiments.

Preparation of leaf extract: Few healthy leaves (*T. portulacastrum* and *M. oppositifolia*) were collected and about 10 g leaves were washed multiple times in faucet water and flushed well. Distilled water (100 mL) was added to the cup containing small pieces of leaves. It was then warmed at 80 ºC for 25 min and filtered.

Synthesis ZnO NPs by chemical method: Zinc nitrate (0.2 M) solution was prepared in 100 mL of deionized water and added dropwise to the prepared leaf extract (10 mL) after 10 min. This proceeded until its pH arrived at 10 and the solution was blended persistently for 2 h. At that point it was shifted for the time being and dried futile. The accomplished powder was determined in a stifle heater at 400 ºC for 4 h. The eventual outcome was recognized as ZnO nanoparticles.

Biosynthesized ZnO nanoparticles: Zinc nitrate (0.2 M) solution was prepared in 100 mL of deionized water. The leaf extract (10 mL) was added at 85 ºC for 4 h and stirred continously. The formation of nanoparticles was observed by the visual shade of yellowish coloured, which further turn to purple solution. Further, the solution was dried at 400 ºC for 4 h and the subsequent powder was additionally exposed to further studies.

Characterization: Shimadzu 6000 X-ray diffractometer (KUA radiation (Kα = 1.5406 Å) was operated at room temperature with crystal phase XRT analysis. The optical absorption spectrum was recorded using a Jasco V-670 spectrophotometer in the 300-800 nm range. Photoluminescence studies were performed by Chlorolog 3-Horiba Jobin Yuen at room temperature with an excitation wavelength of 325 nm. Nanoparticle morphology was studied by SEM and HR-TEM (Hitachi S-4500 SEM engine). Perkin-Elmer IR spectrophotometer using a KBr pallets at room temperature in the 4000-400 cm^{-1} range with a scanning rate of 4 cm^{-1}/min was used to identify groups in the synthesized nanoparticles.

Photocatalytic activity: The photocatalytic properties of synthesized nanoparticles was carried out by using acid black 1 dye under sunlight radiation. The dye solution was prepared by dissolving 10 mL of dye in 500 mL of water. Prior to illumination, the suspension of synthesized nanoparticles (0.06 g in 100 mL of dye solution) was stirred in the dark for 60 min. Once the solution was equilibrated, the suspension was placed in a domestic sunlight furnace for approximately 75 min, turning a dark orange colourless solution. The concentration of acid black 1 dye in the samples was intentional using an UV-visible spectrophotometer.

Antibacterial activity: Kirby Bauer diffusion method was applied to evaluate the antibacterial properties of leaf extracts (*T. portulacastrum* and *M. oppositifolia*) and synthesized ZnO nanoparticles [12]. The liquid supplement was suspended with microorganisms on the agar and filled plate utilizing sterile wells with sterile cotton fabric and made with the assistance of a sterile steel sterile stopper drill. Samples (50 and 100 µL) were added to the aseptic state in the well and 25 µg of ciprofloxacin was utilized as control. The test plates were brooded at 35 ºC for 24 h, after which the square breadth was estimated and noted in terms of mean zone millimeters.

Antioxidant activity

DPPH free radical assay: The effect of leaf extract (*T. portulacastrum* and *M. oppositifolia*) and synthesized ZnO NPs on DPPH radical were estimated according to the reported method [12]. Various concentrations of 25, 50, 100, 125, 250 and 500 µg/mL of the test solution was added to 0.1 mM of methanolic DPPH solution, and then the soultion was incubated for 60 min at room temperature under dark conditions. The absorbance of the solution was measured spectrophotometrically at 517 nm. Ascorbic acid was used as standard reference.

Nitric oxide scavenging activity: The absorbance of nitric oxide produced from sodium nitroprusside (pH 7.3) was measured at 546 nm mixed with the aqueous leaf extract (*T. portulacastrum* and *M. oppositifolia*) and both synthesized ZnO nanoparticles (5 mL) of different concentrations (25, 50, 100, 125, 250 and 500 µg /mL) using a SpectraMax Plus UV-Vis microplate reader (Molecular Devices, GA, USA). The percentage nitrite radical scavenging activity of the leaf extracts and synthesized ZnO nanoparticles and gallic acid were calculated using the following formula:

$$\text{Scavenging activity } (\%) = \frac{(A_{control} - A_{sample})}{A_{control}} \times 100$$

where $A_{control}$ and A_{sample} are the absorbance of absence and presence of the samples of extracts or standards.

RESULTS AND DISCUSSION

Structural (XRD) analysis: The XRD spectra of both chemically and biosynthesized ZnO nanoparticles are shown in Fig. 1. The XRD peaks at 31.81º, 34.44º, 36.31º, 47.60º, 56.62º, 63.01º, 66.48º, 67.97º and 69.19º correspond to the (100), (002), (101), (102), (110), (103), (200), (112) and (201) reflection planes indicates the hexagonal Wurtzite structure [13]. No other unwanted peakes were found in the XRD spectra, which indicated that the synthesized nanoparticles are purely formed.

Using Debye-Scherrer′s equation, the size of nanoparticle was determined as follows:

$$D = \frac{0.9\lambda}{\beta \cos\theta}$$

where D is the crystallite size, λ is the wavelength of X-ray source, β is the full width at half maximum, θ is the Bragg′s diffraction angle. The calculated average crystalline size of chemically synthesized ZnO NPs is 21 nm, and reduced to 18 and 15 nm when synthesized ZnO NPs using *T. portulacastrum*

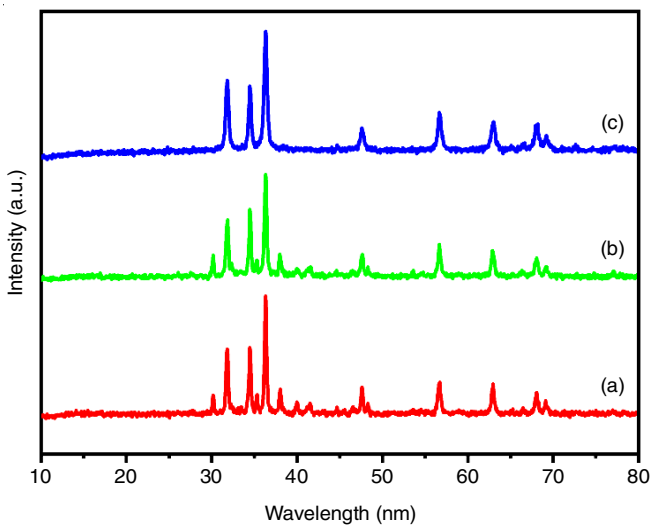

Fig. 1. X-ray diffraction pattern of (a) chemical synthesized ZnO-NPs (b) *T. portulacastrum* and (c) *M. oppositifolia* mediated biosynthesized ZnO-NPs

and *M. oppositifolia* leaf extracts. The crystallinity of bio-synthesized ZnO NPs is less when compared to the chemically synthesized ZnO NPs (Table-1).

The lattice constant (a), dislocation density (δ) and micro-strain (ε) are calculated [5] using the following equations:

$$\frac{1}{d^2} = \frac{4}{3}\left(h^2 + hk + \frac{k^2}{a^2}\right) + \frac{l^2}{c^2}$$

$$\varepsilon = \frac{\beta\cos\theta}{4}$$

$$\delta = \frac{1}{D^2} \text{ line/m}^2$$

Table-1 shows the low microstrain with increase in the translucent size while the less separated thickness for indicates the highcrystallinity of the nanoparticles. Consequently, chemically mediated ZnO NPs shows a high level of surface deformities and deteriorated surface quality, however bio-synthesized ZnO NPs show low of surface imperfections.

Morphological (HR-TEM) analysis: Typical HR-TEM images obtained for both chemically and biosynthesized ZnO NPs are shown in Figs. 2-4. The synthesized nanoparticles show the spherical particles with narrow size distribution. Figs. 2d, 3d and 4d shows that the average particles size 25, 20, 22

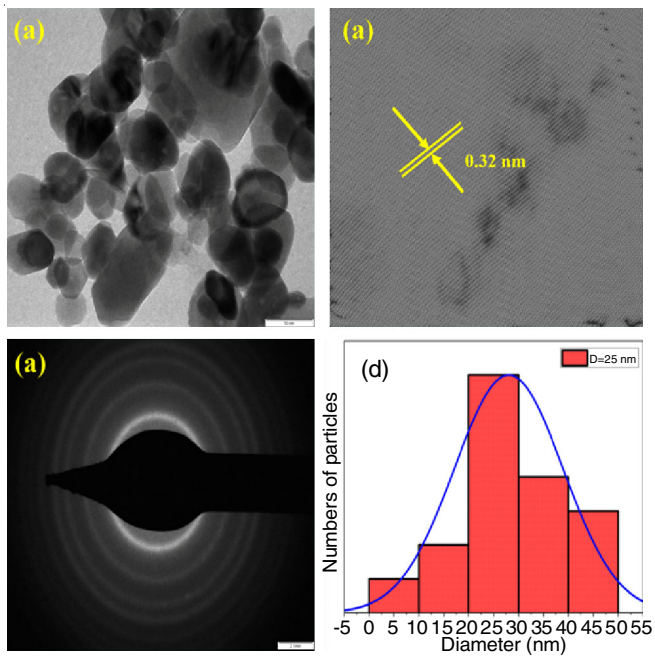

Fig. 2. (a) HR-TEM image (b) lattice fringes c) SAED pattern d) Particle size of chemically synthesized ZnO NPs

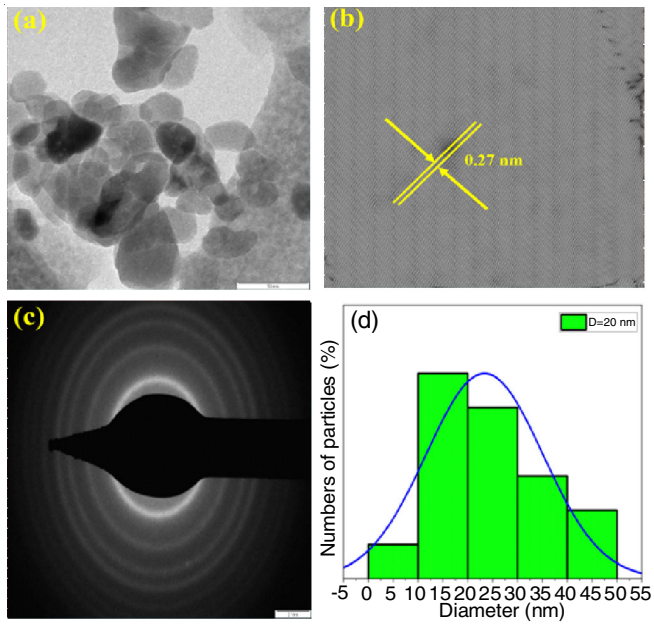

Fig. 3. (a) HR-TEM image (b) lattice fringes (c) SAED pattern (d) particle size of biosynthesized (*M. oppositifolia*) ZnO NPs

TABLE-1
DIFFERENT STRUCTURE PARAMETER OF CHEMICALLY AND BIOSYNTHESIZED (*T. portulacastrum* and *M. oppositifolia*) ZnO-NPs

Samples	2θ	FWHM	Miler indices (hkl)	Average micro strain (ε)	Average dislocation density (δ)	Average crystalline size (D)
Chemically synthesized	36.2647	0.24101	(101)	4.567	7.457	21.41
	31.4780	0.29657	(100)			
	34.5687	0.25678	(002)			
Biosynthesized (*T. portulacastrum*)	36.1547	0.25200	(101)	7.657	14.541	18.89
	31.8971	0.36870	(100)			
	34.5687	0.59780	(002)			
Biosynthesized (*M. oppositifolia*)	36.7890	0.25400	(101)	9.5671	19.023	15.04
	31.8970	0.36870	(100)			
	34.9871	0.29780	(002)			

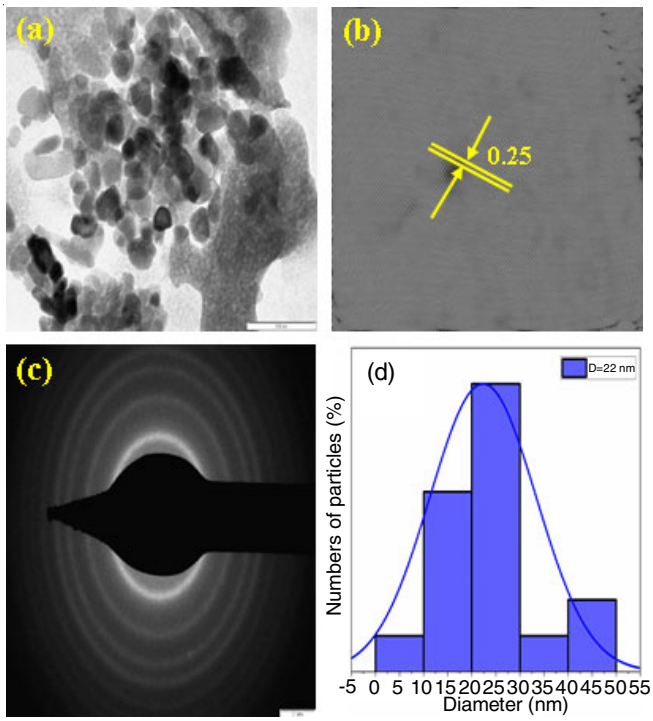

Fig. 4. (a) HR-TEM image (b) lattice fringes (c) SAED pattern (d) particle size of biosynthesized (*T. portulacastrum*) ZnO-NPs

nm for chemically and biosynthesized ZnO-NPs using *T. portulacastrum* and *M. oppositifolia* leaf extract, respectively. *M. oppositifolia* leaf extract used to the biosynthesized ZnO nanoparticles are smaller particles size when compared to the chemically synthesized ZnO NPs and *T. portulacastrum* leaf extract used to the biosynthesized ZnO NPs. Apart from this, 2 nm resolution studies of synthesized samples shows 0.29, 0.25 and 0.21 nm 'd' space, which states the crystalline nature of synthesized nanoparticles. The SAED pattern of synthesized nanoparticles in Figs. 2c, 3c and 4c shows the reflection corresponding to the monoclinic structure and very well matched with the XRD analysis [14].

FT-IR analysis: The existence of metal oxygen bonding and other functional group of synthesized nanoparticles were analyzed by using FT-IR spectroscopy. Fig. 5 shows that the FT-IR spectra of aqueous leaf extract of *M. oppositifolia* and *T. portulacastrum*, chemically and biosynthesized ZnO NPs observed in the wave number range of 4000 to 400 cm^{-1}. In the FT-IR spectrum of *M. oppositifolia* and *T. portulacastrum*

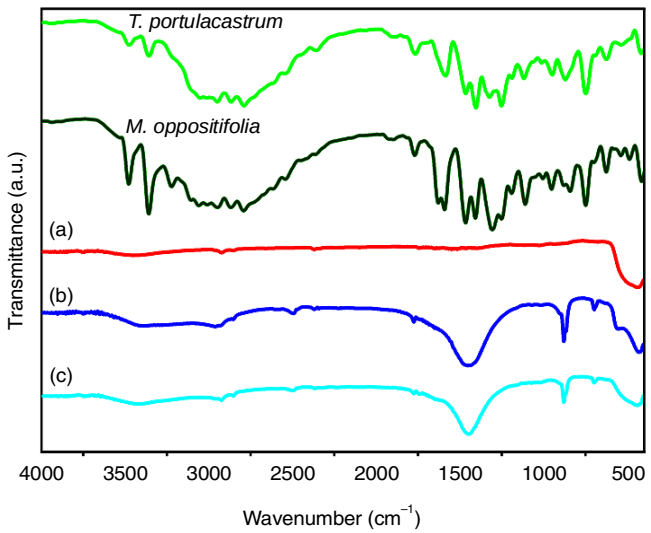

Fig. 5. FT-IR spectra of *M. oppositifolia* and *T. portulacastrum* leaf extract; (a) chemically synthesized ZnO NPs; b-c) biosynthesized (*M. oppositifolia* and *T. portulacastrum* leaf extract) ZnO NPs

leaf extracts, the peak at 2943.57 cm^{-1}, showed C-F *str*. and C-O *str* of alkyl halides and alcohols, respectively [13].

A band at 3423.4 cm^{-1} indicated C=O *str.* of acyl chloride, while peaks at 1542.8 cm^{-1} represent the N-H *str.* of aromatic 2º amine and C-N *str.* of aromatic groups, respectively. These functional groups correspond to alkaloids, flavonoids, phenols, carbohydrates and saponis present in the aqueous leaf extract of *M. oppositifolia* and *T. portulacastrum* are given in Table-2. The FT-IR spectrum of chemically synthesized ZnO-NPs, the peak at 3495.09 cm^{-1} showed free O-H bonding [15] and 2945.21 cm^{-1} showed symmetric and asymmetric stretching vibrations. A band at 2740.56 cm^{-1} indicated aromatic benzene structure, while the peak at 2498.04 cm^{-1} represented the C–H stretching [5]. In biosynthesized (*M. oppositifolia* and *T. portulacastrum*) ZnO NPs, two extra peaks were observed around 3689.04 cm^{-1} (O-H vibration) and 2895.23 cm^{-1} (C-H vibration), which showed the influence of leaf extract [12]. Additional peaks around 700 and 596 cm^{-1} shows the impact of leaf extract, which is absent in the chemical mediated ZnO NPs. However, in case ZnO NPs from *T. portulacastrum*, a shift of peak to a lower region is due to the association of leaf extract with zinc oxide during mixing to a greater extent. These phytochemicals go about as a holding surface to ZnO-NPs and it settles ZnO-NPs by electron adjustment [5].

TABLE-2
FUNCTIONAL GROUP AND COMMONLY ASSIGNED COMPONENT OF CHEMICALLY AND BIOSYNTHESIZED (*M. oppositifolia* AND *T. portulacastrum* LEAF EXTRACT) ZnO NPs

Wavenumber (cm^{-1})			Functional group and commonly assigned component
Chemically synthesized ZnO NPs	Biosynthesized ZnO NPs		
	M. oppositifolia	*T. portulacastrum*	
3495.09	3487.12	3465.47	Free O-H bonding
2945.21	2956.24	29547.10	Symmetric and asymmetric stretching vibration
2740.56	2756.28	2738.58	Aromatic benzene structure
2498.04	2484.56	2487.56	C–H stretching
1401.58	1456.78	1423.41	C–C stretching vibrations
–	756.07	76396	C–H vibrations
–	596.07	591.56	C=O stretch

Optical analysis: The optical properties of chemically and biosynthesized ZnO NPs were evaluated by UV-Vis diffuse reflectance spectroscopy (DRS) between the wavelength 200 to 800 nm and room temperature. The UV-vis DRS spectrum of as synthesized ZnO NPs is shown in Fig. 6, which reflects the absorption edges of chemical and biosynthesized ZnO NPs at about 365, 378 and 382 nm, respectively. Biosynthesized ZnO NPs exhibited surface plasmon resonance peaks at 378 and 382 nm, which is a red shift [16]. Bandgap energy of chemically and biosynthesized ZnO NPs were found to be 37.42, 3.34 and 3.49 eV (Fig. 7), which revealed that optical band gap energy of *M. oppositifolia* leaf extract mediated ZnO NPs shows very low compared to chemically and *T. portulacastrum* plant mediated ZnO NPs. In the UV region, strong absorption showed that the biosynthesized ZnO NPs have a good capacity for UV protection applications.

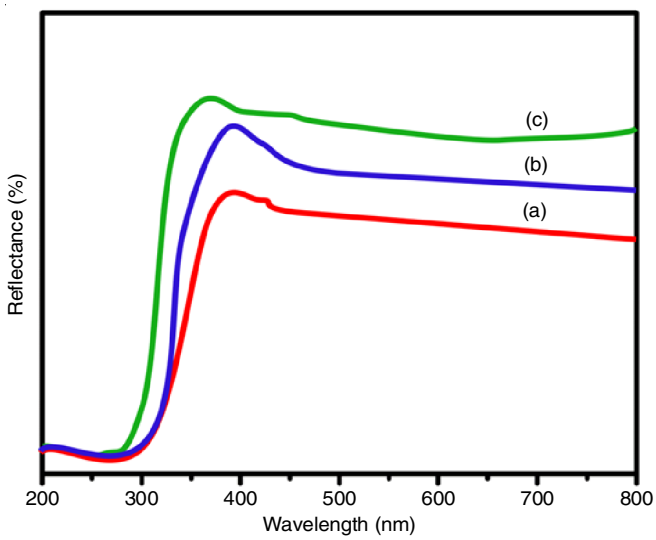

Fig. 6. UV-Vis DRS spectra of (a) chemically synthesized ZnO-NPs and (b-c) biosynthesized (*M. oppositifolia* and *T. portulacastrum* leaf extract) ZnO-NPs

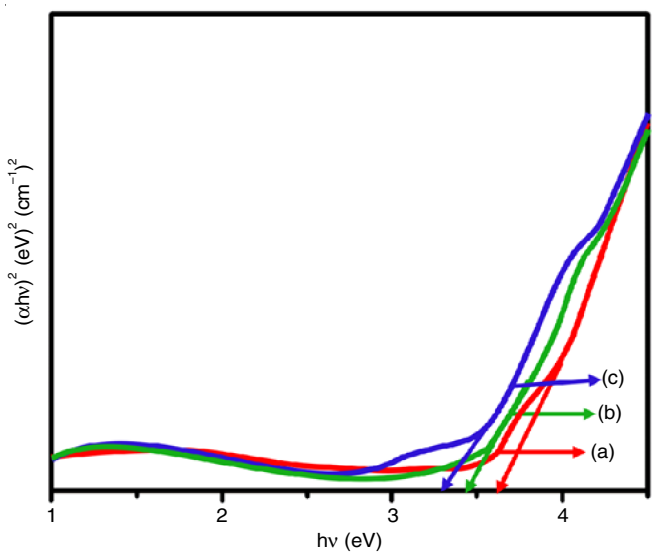

Fig. 7. Band gap energy of chemically synthesized ZnO-NPs and biosynthesized (*M. oppositifolia* and *T. portulacastrum* leaf extract) ZnO-NPs

Photoluminescence (PL) analysis: PL spectra of chemical and biosynthesized ZnO NPs are shown in Fig. 8. The PL spectrum of ZnO NPs usually comprises two major emissions peaks, one near the band edge and the next one visible by the low-emission band [17]. For chemically synthesised ZnO-NPs, usually associated with Zn defects, such as transitions from Zn levels to valence belt statements as shown in Fig. 8a, the maximum blue emission width centred at 562 nm can be observed. The photoluminescence spectrum of biosynthesized ZnO NPs using *M. Opositifolia* and *T. portulacastrum* are shown in Fig. 8b-c. It consists of two peaks, a weak UV band at 423 nm and an intense orange band at 558 nm.

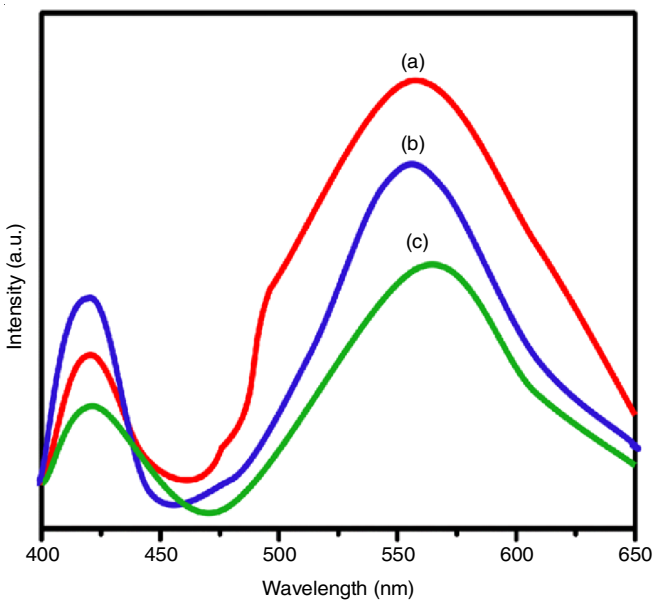

Fig. 8. PL spectra of chemically synthesized ZnO NPs and biosynthesized (*M. oppositifolia* and *T. portulacastrum* leaf extract) ZnO NPs

The PL emission is associated with the close-band transition, the exciting collision and the recombination of free-exciton. UV emissions are responsible for changes in the valence band of Zn, while yellow-orange emissions are generally attributed to DLE bands and excess oxygen, *i.e.* transitions between the vacancy and neutral and single charged oxygen intermediates [18]. Receptor-like (Oi) defects can be created easily in N-type ZnO, so the transition from different energy sources is possible. Yellow-orange fluorescent materials are widely used for optical and medical treatment, and fluorescent nano-products with bio-applications have become increasingly popular in recent years. During chemical interactions between plant extract and ZnO NPs, some defects can be concluded that this affects the density and the emission properties. As mentioned earlier, leaf extract contains antioxidants (such as phenols, flavonols, *etc.*) bind to ZnO NPs through their carboxylic groups, which can create new conditions or defects in the band spacing of host structure and, ultimately, affect ZnO emissions.

Photocatalytic activity: Photocatalytic activity of chemically and biosynthesized ZnO NPs were carried out in the presence of the open sunlight using acid black 1 dye. The degradation of acid black 1 dye was estimated various time intervals 0, 15, 30, 45, 60, 75 min. The UV-Vis absorption peak at 632 nm refers to

the colour of acid black 1 dye reduced from dark blue to colourless by the electron transfer process. After 75 min, chemically synthesised ZnO NPs have degraded an insignificant amount of the dye, while biosynthesized ZnO NPs shows higher degradation efficiency. This is anticipated due to presence of defects and oxygen vacancies created by leaf extract inside the ZnO NPs. Table-3 shows that biosynthesized (*T. portulacastrum*) ZnO NPs has exhibited a maximum degradation of 96% compared with the chemically synthesized ZnO NPs and *M. oppositifolia* leaf extract mediated ZnO NPs.

TABLE-3
EFFECT OF ACID BASED 1 DYE DEGRADATION OF CHEMICALLY AND BIOSYNTHESIZED (*M. oppositifolia* AND *T. portulacastrum* LEAF EXTRACT) ZnO NPs

Time (min)	Degradation of dye (%)		
	Chem ZnO-NPs	Bio (1) ZnO-NPs	Bio (2) ZnO-NPs
0	0	0	0
15	15	24	26
30	21	35	38
45	36	57	50
60	48	68	71
75	62	80	83
90	78	94	96

This is comprehensible because of the physical deficiencies and increased cation oxidant levels. The literature described this phenomenon previously as a trapping foundation for holes and electrons in excess of cation produced during the stimulant process [5]. Biosynthesized ZnO NPs act similarly to electron holes, resulting in significantly enhancing the separation of electron-hole pairs formed by photo illumination and preventing their recombination as a result of enhanced photocatalytic activity [12].

Mechanism of photocatalytic activity: The reason of the improved photocatalytic action for biosynthesized ZnO NPs, it expands the surface area through surface opening [19,20]. The photo-catalytic system of semiconductor materials proceeds with the arrangement of electron-gap sets (e^-, hv^+) and resulting partition and reconnection of electrons and openings. The photocatalytic activity of artificially incorporated ZnO NPs is credited to the benefactor states brought about by an enormous number of imperfection sites, for example, oxygen and interstitial zinc particles and to the acceptor states, which emerge from zinc opening and interstitial oxygen molecules. However, biosynthesized ZnO NPs for the degradation of acid black 1 dye under sunlight illumination, at first electron-hole sets are made and afterward the species, for example, $^{\bullet}OH$ and $O^{\cdot 2-}$ are formed [5].

Kinetics analysis: The photodegradation of acid black 1 dye by chemically and biosynthesized ZnO NPs were also investigated kinetically and the results are shown in Fig. 9a. The predictable (K) rate of acid black 1 decrease with mixed nanoparticles is fixed, as demonstrated by the condition of the pseudo-first order rate. The light-time portion graph $\ln(C_o/C_t)$ provides stable rates of 1.671 and 1.977 min^{-1}. The corresponding ratio coefficient (R^2) is also determined to be 0.983 and 0.982 for ZnO NPs and biosynthesized ZnO-NPs. Finally, it is presumed that C_o/C_t is reduced over time and that the level of discolouration increased over time (Fig. 9b). The conclusion of this photocatalysis experiment clearly shows that phytochemicals present in the leaf extract improve the photocatalytic activity of ZnO NPs to some extent.

Antibacterial activity: The Gram-positive strains (*Bacillus subtilis*, *Staphylococcus saprophyticus*) and Gram negative (*Escherichia coli* and *Pseudomona aeruginosa*) inibition area is investigated with chemically and biosynthesized ZnO NPs in the concentration of 50 and 100 µg. Obviously the biosynthesized ZnO NPs restrain the development of both Gram-negative and Gram-positive microbes (Figs. 10 and 11). The results of chemically and biosynthesized ZnO NPs are shown in Table-4. It is found that biosynthesized ZnO NPs restricted the development of both Gram-negative and Gram-positive microbes, which is due to a decrease in their band gap. Due to the decrease in band gap, the excitation of electron is likely to be created.

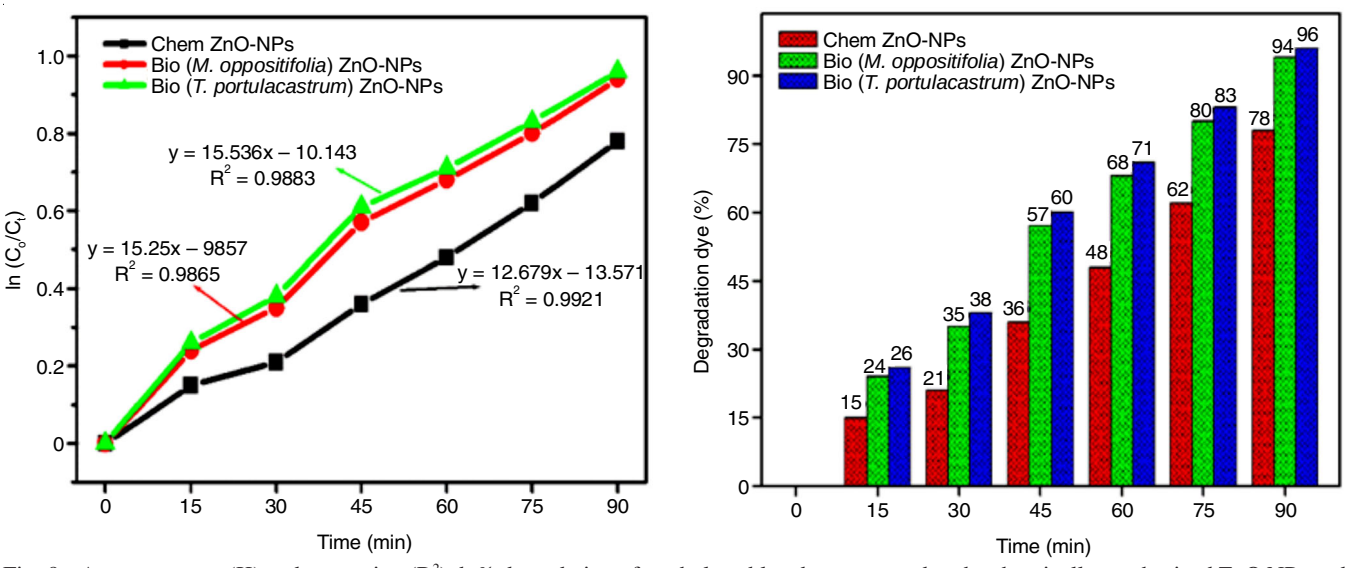

Fig. 9. A rate constant (K) and regression (R^2); b % degradation of methylene blue dye compared to the chemically synthesized ZnO NPs and biosynthesized (*M. oppositifolia* and *T. portulacastrum* leaf extract) ZnO NPs

TABLE-4
ANTIBACTERIAL ACTIVITY OF *M. oppositifolia* AND *T. portulacastrum* LEAF EXTRACT; (a) CHEMICALLY SYNTHESIZED ZnO-NPs; (b-c) BIOSYNTHESIZED (*M. oppositifolia* AND *T. portulacastrum* LEAF EXTRACT) ZnO-NPs AT 50 µL AND 100 µL

Bacteria	Zone of inhibition											
	50 µL						100 µL					
	Leaf 1	Leaf 2	Chem	Bio1	Bio2	St	Leaf 1	Leaf 2	Chem	Bio1	Bio2	St
Bacillus subtilis	--	1	3	8	9	15	6	7	12	19	20	25
Staphylococcus saprophyticus	2	1	4	7	7	15	7	8	13	17	19	25
Pseudomonas aeruginosa	2	2	5	9	10	16	8	8	15	20	22	25
Escherichia coli	3	2	4	10	11	17	10	11	17	18	20	26

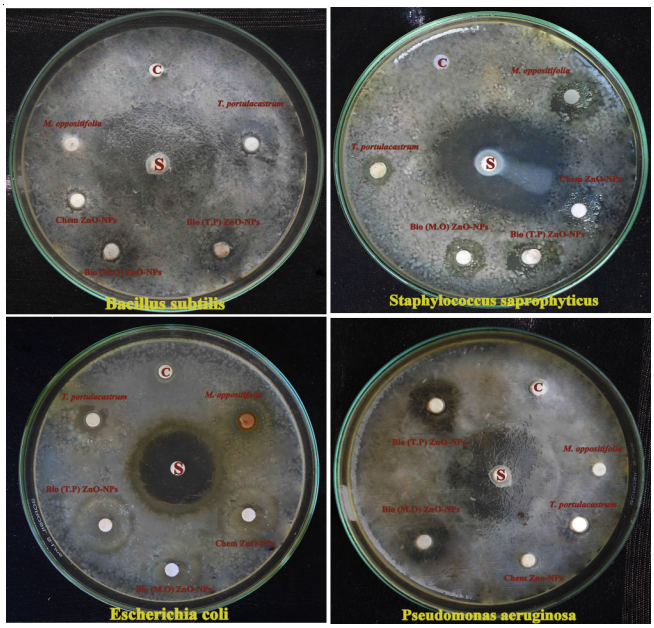

Fig. 10. Antibacterial activity of *M. oppositifolia* and *T. portulacastrum* leaf extract; (a) chemically synthesized ZnO NPs; (b-c) biosynthesized (*M. oppositifolia* and *T. portulacastrum* leaf extract) ZnO NPs at 50 µL

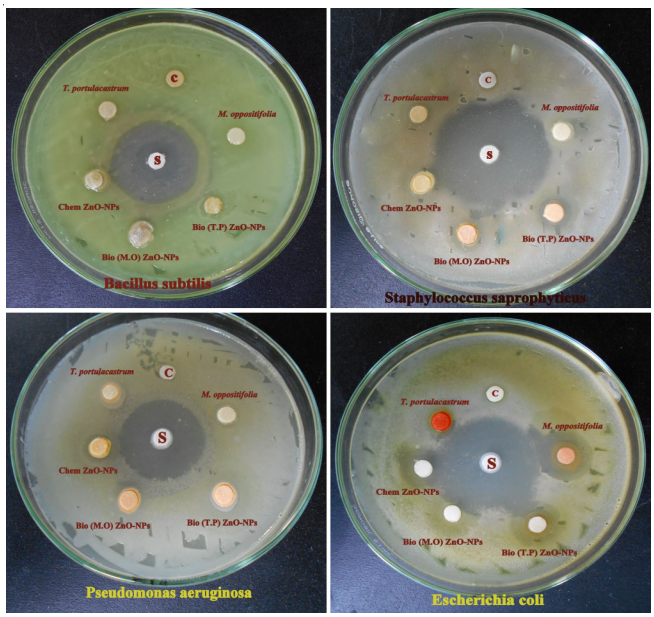

Fig. 11. Antibacterial activity of *M. oppositifolia* and *T. portulacastrum* leaf extract; (a) chemically synthesized ZnO NPs; (b-c) biosynthesized (*M. oppositifolia* and *T. portulacastrum* leaf extract) ZnO NPs at 100 µL

Generally, it improves the photocatalytic activity and also to improve bacterial action of ZnO NPs. In addition, due to the distinctive surface interface properties, there could be various physical properties, the potential for assimilation dissolvability towards the path to microbes, affirming various antibacterial effects [21].

The interaction between the blended nanoparticles and the cell wall of microorganisms was changed because of phyto-chemicals of leaf extract. The evolution of *E. coli* and the other two microorganisms have been influenced by the biosynthesized ZnO NPs in contrast to chemically synthesized ZnO NPs. This differentiation in bacterial action of biodegradable ZnO NPs′s against Gram-negative and Gram-positive strains may be due to cell wall structure of the specific microscopic organisms.

Essentially, the bactericidal action of chemically and biosynthesized ZnO nanoparticles depends mainly on the degree of reactive oxygen species (ROS) and single oxygen. This is mainly due to the increased sites of oxygen vacancies and the diffusion capacity of the reaction particles within the nanoparticles. In addition, the presence of nanoparticles on the outside of microbes or cytoplasms can disrupt cell capacity and cause the formation of cell layers. Results have shown that the biosynthesized ZnO NPs could be a promising opportunity for potential drug conveyance strategies to address some critical diseases later on.

Antioxidant activity: The impact of antioxidants on DPPH is thought to be due to their hydrogen donation activity [5]. As DPPH is considered a lipophilic radical, it instantly accepts electrons from the antioxidant compound and changes its colour from violet to yellow. Therefore, DPPH accepts a constant free radical and an electron or hydrogen intensity as a constant dynamic molecule. The results on the effect of different concentrations of chemically, biosynthesized ZnO NPs and ascorbic acid on DPPH radical scavenging activity is shown in Fig. 12a.

At concentration 25-500 µg/mL, *M. oppositifolia* leaf extract showed scavenging rate ranging from 14% to 45%, *T. portulacastrum* leaf extract showed 15% to 48%, chemically ZnO NPs showed 22% to 71%, *M. oppositifolia* mediated biosynthesized showed 26% to 89%, *T. portulacastrum* used biosynthesized 28% to 91% and standard ascorbic acid showed 31% to 96%. Compared to the leaf extracts (*M. oppositifolia* and *T. portulacastrum*), chemically and biosynthesized ZnO-NPs, ascorbic had the highest radical scavenging activity with the lowest IC_{50} µg/mL (116.42). *M. oppositifolia* and *T. portulacastrum* leaf extracts had the lowest radical scavenging activity with the highest IC_{50} µg/mL (173.06 and 170.54). Chemically synthesized ZnO NPs shows 141.40 and biosynthesized ZnO NPs

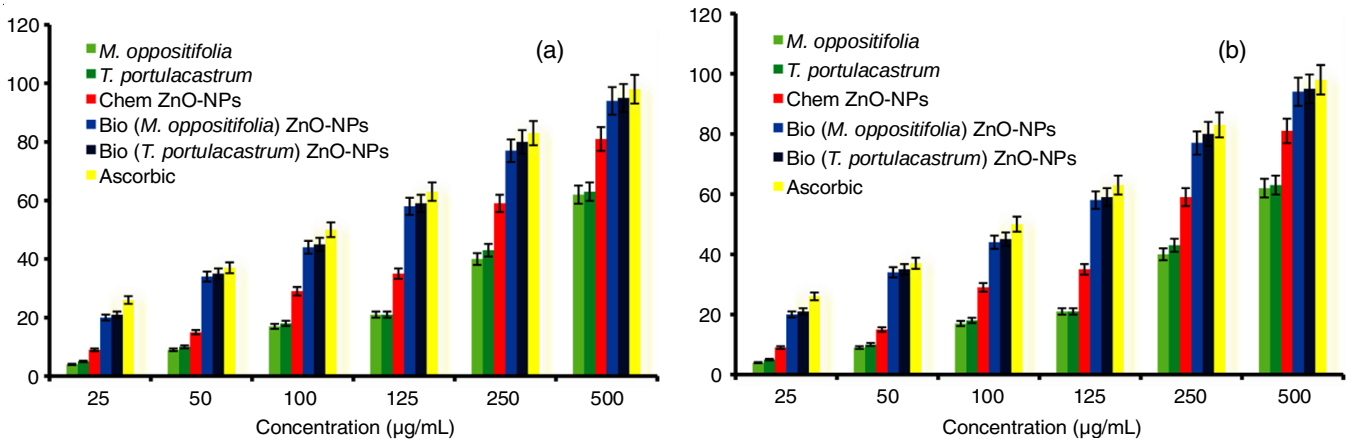

Fig. 12. (a) DPPH free radical; (b) nitric oxide scavenging activity of *M. oppositifolia* and *T. portulacastrum* leaf extract; Chemically synthesized ZnO-NPs; and biosynthesized (*M. oppositifolia* and *T. portulacastrum* leaf extract) ZnO NPs

showed moderated scavenging activity with IC_{50} µg/mL (123.83 and 121.04), the lower IC_{50} µg/mL values reflect the greater potency for antioxidant activity of the samples. The results for DPPH free redical scavenging activity (IC_{50} µg/mL) of leaf extract, chemically, biosynthesized ZnO-NPs and standard, produced by different concentration are presented in Table-5.

Nitric oxide scavenging activity: The percentage of nitric oxide scavenging activity of 25-500 µg/mL of chemically synthesized ZnO-NPs shows 15% to 81%, *M. oppositifolia* and *T. portulacastrum* leaf extract shows 4% to 62% and 5% to 63% and biosynthesized ZnO NPs shows 34% to 94% and 21% and 95%, respectively. *M. oppositifolia* and *T. portulacastrum* leaf extracts had the lowest radical scavenging activity with the highest IC_{50} µg/mL (177.25 and 173.56) (Fig. 12b). Chemically synthesized ZnO NPs shows 151.04 and biosynthesized ZnO NPs showed moderated scavenging activity with IC_{50} µg/mL (125.89 and 120.58). The lower IC_{50} µg/mL values reflect the greater potency for antioxidant activity of the samples. The results for nitric oxide radical scavenging activity (IC_{50} µg/mL) of leaf extracts, chemically, biosynthesized ZnO-NPs and standard, produced by different concentration are presented in Table-6.

For the present study, a higher antioxidant activity was observed in *T. portulacastrum* mediated ZnO NPs, than chemically and biosynthesized ZnO NPs using *M. oppositifolia* leaf extract. Protective capping of ZnO NPs by polyphenols and respective size of the ZnO-NPs as discussed earlier could be the possible reason for the observations made in this experiment. However, to make confident conclusions, in depth analyses are required to elucidate the possible mechanisms underlying the toxicity of chemically synthesized ZnO nanoparticles.

CONFLICT OF INTEREST

The authors declare that there is no conflict of interests regarding the publication of this article.

TABLE-5
DPPH FREE RADICAL ACTIVITY OF *M. oppositifolia* AND *T. portulacastrum* LEAF EXTRACT; CHEMICALLY SYNTHESIZED ZnO-NPs; AND BIOSYNTHESIZED (*M. oppositifolia* AND *T. portulacastrum* LEAF EXTRACT) ZnO-NPs

Concentration	Leaf 1	Leaf 2	Chem ZnO-NPs	Bio (M.P) ZnO-NPs	Bio (T.P) ZnO-NPs	Standard
500	50 ± 0.2	54 ± 0.4	71 ± 0.9	93 ± 0.1	94 ± 0.2	96 ± 0.5
250	27 ± 0.4	28 ± 0.8	55 ± 0.2	75 ± 0.5	77 ± 0.6	81 ± 0.2
125	18 ± 0.8	18 ± 0.1	34 ± 0.1	53 ± 0.3	54 ± 0.1	63 ± 0.6
100	11 ± 0.1	12 ± 0.2	21 ± 0.6	36 ± 0.9	37 ± 0.2	43 ± 0.9
50	5 ± 0.4	5 ± 0.7	15 ± 0.3	26 ± 0.7	26 ± 0.7	31 ± 0.7
25	3 ± 0.5	4 ± 0.9	8 ± 0.4	16 ± 0.2	17 ± 0.6	21 ± 0.5
IC_{50}	173.06	170.54	147.40	123.83	121.04	116.42

TABLE-6
NITRIC OXIDE SCAVENGING ACTIVITY OF *M. oppositifolia* AND *T. portulacastrum* LEAF EXTRACT; CHEMICALLY SYNTHESIZED ZnO-NPs; AND BIOSYNTHESIZED (*M. oppositifolia* AND *T. portulacastrum* LEAF EXTRACT) ZnO-NPs

Concentration	Leaf 1	Leaf 2	Chem ZnO-NPs	Bio (M.P) ZnO-NPs	Bio (T.P) ZnO-NPs	Standard
500	62 ± 0.4	63 ± 0.1	81 ± 0.9	94 ± 0.4	95 ± 0.2	98 ± 0.2
250	40 ± 0.3	43 ± 0.5	59 ± 0.4	77 ± 0.6	80 ± 0.9	83 ± 0.4
125	21 ± 0.9	21 ± 0.4	35 ± 0.4	58 ± 0.9	59 ± 0.4	63 ± 0.7
100	17 ± 0.6	18 ± 0.3	29 ± 0.7	44 ± 0.4	45 ± 0.6	50 ± 0.4
50	9 ± 0.4	10 ± 0.9	15 ± 0.4	34 ± 0.5	35 ± 0.6	37 ± 0.9
25	4 ± 0.6	5 ± 0.6	9 ± 0.6	20 ± 0.1	21 ± 0.1	26 ± 0.6
IC_{50}	177.45	173.25	151.79	125.41	120.65	110.43

REFERENCES

1. K. Nithya and S. Kalyanasundharam, *OpenNano*, **4**, 100024 (2019); https://doi.org/10.1016/j.onano.2018.10.001
2. S. Alamdari, M.J. Tafreshi and M.S. Ghamsari, *Appl. Phys., A Mater. Sci. Process.*, **125**, 165 (2019); https://doi.org/10.1007/s00339-019-2451-x
3. P. Rauwel, M. Salumaa, A. Aasna, A. Galeckas and E. Rauwel, *J. Nanomater.*, **2016**, 5320625 (2016); https://doi.org/10.1155/2016/5320625
4. M.J. Haque, M.M. Bellah, M.R. Hassan and S. Rahman, *Nano Express*, **1**, 010007 (2020); https://doi.org/10.1088/2632-959X/ab7a43
5. A. Muthuvel, M. Jothibas and C. Manoharan, *J. Environ. Chem. Eng.*, **8**, 103705 (2020); https://doi.org/10.1016/j.jece.2020.103705
6. K. Ali, S. Dwivedi, A. Azam, Q. Saquib, M.S. Al-Said, A.A. Alkhedhairy and J. Musarrat, *J. Colloid Interface Sci.*, **472**, 145 (2016); https://doi.org/10.1016/j.jcis.2016.03.021
7. A. Singh, Neelam and M. Kaushik, *Results Phys.*, **13**, 102168 (2019); https://doi.org/10.1016/j.rinp.2019.102168
8. S. Ambika and M. Sundrarajan, *J. Photochem. Photobiol. B*, **149**, 143 (2015); https://doi.org/10.1016/j.jphotobiol.2015.05.004
9. M. Rajeswari, P. Agrawal, G.S. Roopa, A. Akshay Jain and P. Kumar Gupta, *Mater. Today Proc.*, **5**, 20996 (2018); https://doi.org/10.1016/j.matpr.2018.06.491
10. H.Y. Chai, S.M. Lam and J.C. Sin, *AIP Conf. Proc.*, **2157**, 020042 (2019); https://doi.org/10.1063/1.5126577
11. P. Nagaraju, S.H. Puttaiah, K. Wantala and B. Shahmoradi, *Appl. Water Sci.*, **10**, 137 (2020); https://doi.org/10.1007/s13201-020-01228-w
12. A. Muthuvel, M. Jothibas and C. Manoharan, *Nanotechnol. Environ. Eng.*, **5**, 14 (2020); https://doi.org/10.1007/s41204-020-00078-w
13. E.P. Etape, J. Foba-Tendo, L.J. Ngolui, B.V. Namondo, F.C. Yollande and M.B.N. Nguimezong, *J. Nanomater.*, **2018**, 9072325 (2018); https://doi.org/10.1155/2018/9072325
14. N. Boukhenoufa, R. Mahamdi and D. Rechem, *J. Semicond.*, **37**, 113001 (2016); https://doi.org/10.1088/1674-4926/37/11/113001
15. S. Alamdari, M. Sasani Ghamsari, C. Lee, W. Han, H.-H. Park, M.J. Tafreshi, H. Afarideh and M.H.M. Ara, *Appl. Sci.*, **10**, 3620 (2020); https://doi.org/10.3390/app10103620
16. S.S. Mydeen, R.R. Kumar, M. Kottaisamy and V.S. Vasantha, *J. Saudi Chem. Soc.*, **24**, 393 (2020); https://doi.org/10.1016/j.jscs.2020.03.003
17. C.H. Ahn, Y.Y. Kim, D.C. Kim, S.K. Mohanta and H.K. Cho, *J. Appl. Phys.*, **105**, 013502 (2009); https://doi.org/10.1063/1.3054175
18. F. Vatansever, W.C.M.A. de Melo, P. Avci, D. Vecchio, M. Sadasivam, A. Gupta, R. Chandran, M. Karimi, N.A. Parizotto, R. Yin, G.P. Tegos and M.R. Hamblin, *FEMS Microbiol. Rev.*, **37**, 955 (2013); https://doi.org/10.1111/1574-6976.12026
19. M. Naseer, U. Aslam, B. Khalid and B. Chen, *Sci. Rep.*, **10**, 9055 (2020); https://doi.org/10.1038/s41598-020-65949-3
20. V. Ramasamy, V. Mohana and V. Rajendran, *OpenNano*, **3**, 38 (2018); https://doi.org/10.1016/j.onano.2018.04.002
21. A. Muthuvel, M. Jothibas, V. Mohana and C. Manoharan, *Inorg. Chem. Commun.*, **119**, 108086 (2020); https://doi.org/10.1016/j.inoche.2020.108086